


Quantum oscillations and magnetic field induced Fermi surface reconstruction in the charge density wave state of $A_{0.9}\text{Mo}_6\text{O}_{17}$ ($A = \text{Na}, \text{K}$)

H. P. Zhu, M. Yang ^{*}, J. Z. Ke, H. K. Zuo, T. Peng, and J. F. Wang

Wuhan National High Magnetic Field Center and School of Physics, Huazhong University of Science and Technology, 430074 Wuhan, China

Yi Liu and Xiaofeng Xu

Department of Applied Physics, Zhejiang University of Technology, Hangzhou 310023, China

Y. Kohama and K. Kindo

The Institute for Solid State Physics (ISSP), University of Tokyo, Chiba 277-8581, Japan

M. Greenblatt

Department of Chemistry and Chemical Biology, Rutgers University, Piscataway, New Jersey 08854, USA



(Received 25 May 2020; revised 11 November 2020; accepted 15 December 2020; published 30 December 2020; corrected 25 January 2021)

We present a detailed study of the magnetotransport properties of the charge density wave state in quasi-two-dimensional purple bronze $\text{Na}_{0.9}\text{Mo}_6\text{O}_{17}$ under pulsed fields up to 62 T. Pronounced Shubnikov–de Haas (SdH) oscillations of three frequencies have been observed in the field induced charge density/spin density wave state of the present compound. The two slow oscillations are attributed to the reconstructed electron and hole pockets near the M' point of the Brillouin zone (BZ). The highest-frequency oscillations correspond to an orbit occupying 18.1% of the BZ, which is consistent with the hexagonal electron Fermi surface in the normal state. The appearance of the highest-frequency oscillations can be explained by the magnetic breakdown between the electron pockets at the M' point. This magnetic breakdown behavior has also been observed in $\text{K}_{0.9}\text{Mo}_6\text{O}_{17}$ under very high field range up to 80 T. Based on analyses of the high field SdH oscillations, we propose a possible Fermi surface structure of $\text{Na}_{0.9}\text{Mo}_6\text{O}_{17}$.

DOI: [10.1103/PhysRevB.102.235164](https://doi.org/10.1103/PhysRevB.102.235164)

I. INTRODUCTION

Charge density wave (CDW), commonly found in low-dimensional metallic systems, is a striking ground state of significant importance due to the strong coupling between electrons and the crystal lattice [1]. The purple bronzes $\text{AMo}_6\text{O}_{17}$ with $A = \text{Li}, \text{Na},$ and K are a family of typical low-dimensional materials with the presence of abundant properties related to the CDW state [2–7]. The basic concept of CDW in this family is believed to be due to the presence of Peierls instability together with Fermi surface nesting [8], whereas other mechanisms based on strong electron-phonon coupling are also proposed [9–11] in transition metal dichalcogenides [12,13] and high temperature superconducting cuprates [14,15].

The $\text{AMo}_6\text{O}_{17}$ family shares the common stacking layers consisting of MoO_6 octahedral and MoO_4 tetrahedra sandwich structure separated by the alkali ions layer. Depending on the A cation, the three compounds have shown various electronic structures and CDW-related behaviors. Among them, $\text{Li}_{0.9}\text{Mo}_6\text{O}_{17}$ has been reported to be quasi-one-dimensional (quasi-1D) due to the strong anisotropy and exhibits superconductivity [16,17], Luttinger-liquid behavior [18–20],

and first evidence of spin and charge separation according to Tomonaga-Luttinger prediction [21]. On the other hand, $\text{Na}_{0.9}\text{Mo}_6\text{O}_{17}$ (NMO) and $\text{K}_{0.9}\text{Mo}_6\text{O}_{17}$ (KMO) are quasi-two-dimensional (quasi-2D) with almost identical crystal structures except that NMO is monoclinic with $\beta = 89.94^\circ$ and KMO is trigonal with $\beta = 90^\circ$ [22]. The CDW transition occurs at $T_{\text{CDW}} = 110$ K in KMO and 85 K in NMO, resulting in a metal-to-metal transition, respectively [23]. The electronic structure in the normal state of KMO has been calculated by the tight-binding model, revealing the presence of three Fermi surfaces (FSs) (two electron FSs centered at the Γ point and one hole pocket away from the Γ point) [3] and confirmed by angle-resolved photoemission spectroscopy (ARPES) [24]. The combination of the three FSs brings the possibility of the hidden 1D FS nesting which results in CDW transition at low temperature, gapping out most of the FSs with only very small portions remaining [shown in Fig. 1(c)]. A recent study has reported the discovery of the unconventional enhanced surface CDW state and proposed the new candidate of the electron-electron mediated CDW system [25]. A reinvestigation of the theoretical calculation of the CDW in KMO has been made and puts forward a deeper understanding of the gap opening and FS development in the CDW state [26]. So far, however, there has been little discussion about the electronic structure and CDW phase in NMO. Early FS topology studies revealed by the ARPES had

^{*}ming_yang@hust.edu.cn

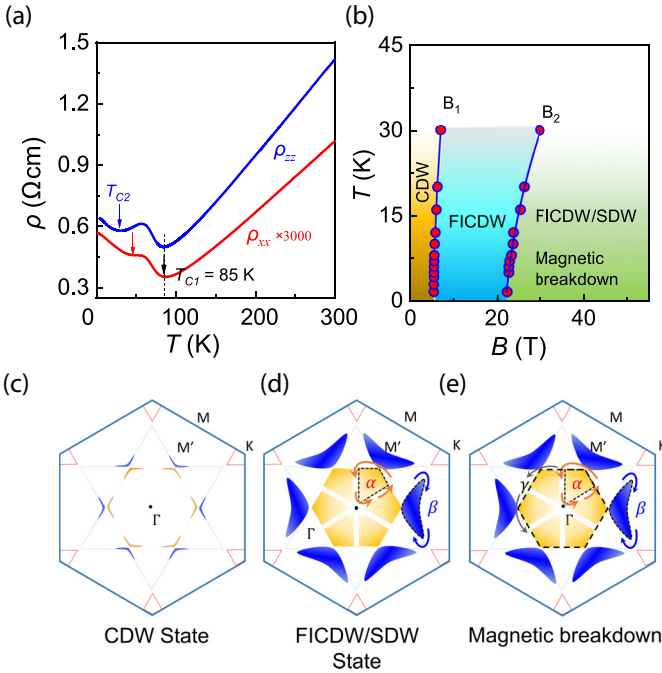


FIG. 1. (a) Temperature dependence of the in-plane and out-of-plane resistivity of NMO. (b) The temperature–magnetic field phase diagram of NMO extracted from the ρ_{zz} measurements. (c) The FS structure of NMO in the CDW state. The blue and gold Fermi arlike pockets are the remaining electron-hole pockets based on the ARPES measurements of KMO [25]. (d) The illustrative FS structure of NMO under magnetic field. The pockets corresponding to the SdH oscillations of F_α and F_β are enlarged due to the reduced CDW gap under magnetic field. (e) The magnetic breakdown under very high magnetic field. The six discrete α electron pockets break down into a much larger orbit γ which is consistent with the original electron band in the normal state.

attained controversial conclusions on whether NMO has a similar FS structure with KMO. Breuer *et al.* [27] reported that NMO has only one electron and one hole band and Gweon *et al.* [28] claimed that NMO and KMO electronic structures are identical. The most recent work by Glans *et al.* [29] then revealed the presence of two electron bands in KMO, but with different rotation symmetry.

Besides the direct determination of the FSs through ARPES, the magnetotransport study provides another approach to study the electronic structures by analyzing the Shubnikov–de Haas oscillations and Hall effect. In this paper, we present the first comprehensive studies of the high-field magnetotransport properties of NMO under magnetic field up to 62 T and at low temperatures ($T < T_{CDW}$). The in-plane longitudinal and Hall resistivity, as well as the out-of-plane resistivity have been systematically studied. The high-field resistivities exhibit pronounced quantum oscillations, which enable the determination of the FSs and related parameters. Based on the results, we demonstrate that the electronic structure of NMO is similar to KMO but more complicated due to the crystallographic structure difference between the two compounds.

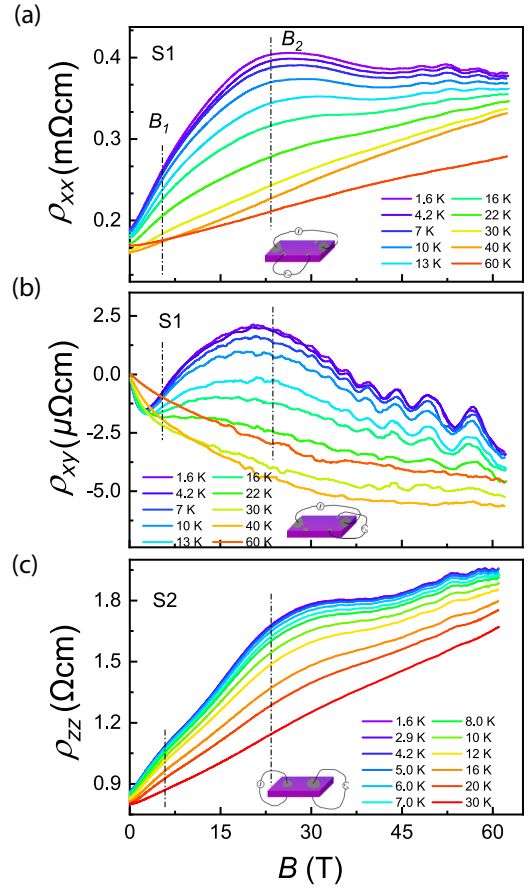


FIG. 2. The magnetotransport properties of $\text{Na}_{0.9}\text{Mo}_6\text{O}_{17}$. (a) and (b) show the ρ_{xx} and ρ_{xy} of S1 as a function of magnetic field up to 62 T, which were measured simultaneously and symmetrized by up and down fields measurements. (c) shows the ρ_{zz} as a function of the magnetic field of S2. The insets of each panel illustrate the measurement configurations of the data.

II. EXPERIMENT

The studied single crystals of NMO were grown by gradient flux technique [30], while KMO were grown by electrolytic reduction method [7]. The plateletlike samples were cleaved and cut into bar shapes of appropriate geometry for in-plane and out-of-plane transport measurements. The in-plane transports, i.e., the longitudinal resistance (R_{xx}) and Hall resistance (R_{xy}), were carried out simultaneously using a five-probe configuration with electrodes made by gold wires and silver paste [shown in the insets of Figs. 2(a) and 2(b)]. The out-of-plane resistance (R_{zz}) was measured using two pairs of electrodes attached to the top and bottom surface of the sample as shown in the inset of Fig. 2(c). Since the sample surfaces are extremely sensitive to the air exposure, two pieces of NMO crystals, named as S1 ($0.8 \times 0.5 \times 0.02$ mm³) and S2 ($2 \times 1 \times 0.1$ mm³), were cleaved for the in-plane and out-of-plane measurements, respectively. The measurements were performed in pulsed magnetic fields up to 62 T with the pulse duration of 150 ms at Wuhan National High Magnetic Field Center [7]. The 80 T shot was realized by a dual-coil magnet with longer duration time of 300 ms. The contact resistances were maintained to be smaller than 1 Ω at low temperatures.

AC currents of 18 mA at 100 kHz were applied for good signal-to-noise ratio with negligible heating effect during the pulses [31]. The R_{xx} (R_{xy}) were measured in positive and negative field directions and the data shown were symmetrized to eliminate the unexpected R_{xy} (R_{xx}) components brought by the imperfect sample symmetry.

III. RESULTS AND DISCUSSION

Figure 1 shows the temperature dependence of the in-plane (sample S1) and out-of-plane (sample S2) resistivity in the temperature range 2–300 K. The in-plane and out-of-plane resistivity show similar behavior, except a large anisotropy over 3000, in line with previously reported values in the literature [23]. Both ρ_{xx} and ρ_{zz} show a linear decrease as the temperature is decreased, showing a metallic behavior at high temperature until an upturn occurs at $T_{C1} = 85$ K. The upturn is attributed to a CDW transition in this compound, where the nested Fermi surfaces are gapped out [29], leading to a metal-to-metal transition. Below T_{CDW} , there exists another upturn (marked by arrows) after a broad maximum around 30–50 K, consistent with the results reported in Ref. [22]. A second CDW transition or a spin density wave (SDW) transition has been suggested for the origin of this second upturn; however, it is still under debate. The slightly different temperatures of the second upturn between the in-plane and out-of-plane resistivity are likely due to the different scatterings in both the in-plane and out-of-plane directions.

Figures 2(a)–2(c) show the ρ_{xx} , ρ_{xy} , and ρ_{zz} at various temperatures and for magnetic field applied normal to the two-dimensional plane of the sample up to 62 T, respectively. We note that only the data during the down-sweep of the pulsed fields are shown in Fig. 2. The low-field ρ_{xx} are in good agreement with that measured in steady magnetic field (0–12 T) [32]. Two transitions can be clearly observed at B_1 and B_2 on ρ_{xx} , which are similar to the anomalies in $\text{K}_{0.9}\text{Mo}_6\text{O}_{17}$ [7]. Pronounced Shubnikov–de Haas (SdH) oscillations become clearly visible at around 35 T and faster-frequency oscillations show up to superimpose when the field is higher than 58 T. The ρ_{xy} shown in Fig. 2(b) are much more complicated than linear, which is typical evidence for the coexistence of multielectron and hole bands. In stark contrast to the holes domination in KMO [7], the ρ_{xy} of NMO is predominantly negative and only turns to positive at intermediate magnetic field range when the temperature is low. As the temperature increases, the bumplike behavior in ρ_{xy} disappears and ρ_{xy} only shows a negative sublinear curve at high temperatures. Furthermore, additional SdH oscillations with a much slower frequency have been found in the high-field range. Figure 2(c) shows the out-of-plane ρ_{zz} measured in sample S2 at various temperatures. As can be seen, $\rho_{zz}(B)$ shows similar magnetic transitions at B_1 and B_2 . The magnetoresistivity, defined as $\text{MR} = \frac{\rho(B) - \rho(0)}{\rho(0)} \times 100\%$, reaches 100% for ρ_{zz} at the saturation field, which is exactly the same with the MR for ρ_{xx} . SdH oscillations are also observed on the positive background in high magnetic field range.

In order to reveal the electronic structure and address the contribution of different bands, we now turn to the quantitative analysis of the quantum oscillations. By subtracting a polynomial background at 1.6 K $< T < 40$ K, we extract

the oscillatory parts of ρ_{xx} , ρ_{xy} , and ρ_{zz} . Figures 3(a), 3(b), and 3(c) present the $\Delta\rho_{xx}$, $\Delta\rho_{xy}$, and $\Delta\rho_{zz}$ as a function of magnetic field in the high-field range and at various temperatures. As can be clearly seen, the oscillation amplitudes systematically decrease as the temperature increases and vanish at around 40 K, consistent with the conventional SdH oscillations. The three $\Delta\rho$ at the lowest temperature ($T = 1.6$ K) as a function of inverse magnetic field $1/B$ are plotted in Fig. 3(d). $\Delta\rho_{xy}$ shows an almost perfect $1/B$ periodicity, while in $\Delta\rho_{xx}$ and $\Delta\rho_{zz}$ the oscillation patterns are complex with more than one period. Since the frequencies of the SdH oscillations are intimately related to the electronic populations, we performed fast Fourier transforms (FFT) on $\Delta\rho_{xx}$, $\Delta\rho_{xy}$, and $\Delta\rho_{zz}$, respectively. The FFT spectra of the three datasets at 1.6 K are compared in Fig. 3(e). The FFT of $\Delta\rho_{zz}$ apparently reveals three main peaks at $F_\alpha = 386 \pm 5$ T, $F_\beta = 574 \pm 12$ T, and $F_\gamma = 2779 \pm 20$ T, indicating that at least three different electronic bands are involved. Meanwhile, F_β and F_γ can be identified in $\Delta\rho_{xx}$ while only F_α in $\Delta\rho_{xy}$. The different frequencies between $\Delta\rho_{xx}$ and $\Delta\rho_{xy}$ suggest that oscillations are dominated by bands with different mobilities and they are all responsible for the SdH oscillations in $\Delta\rho_{zz}$. Through the usual Onsager relation $F = \hbar/(2\pi e)S_F$ with \hbar is the reduced Planck constant and e is the elementary charge [33], we can determine the S_F which is the extremal cross-sectional area of the Fermi surface perpendicular to the magnetic field. From the above frequencies, we calculate that $S_\alpha = 3.68 \times 10^{-2} \text{ \AA}^{-2}$, $S_\beta = 5.5 \times 10^{-2} \text{ \AA}^{-2}$, and $S_\gamma = 2.65 \times 10^{-1} \text{ \AA}^{-2}$, which occupy 2.52%, 3.75%, and 18.1% of the undistorted hexagonal Brillouin zone (BZ) in the normal state, respectively.

The cyclotron mass (m_c) can be deduced from the temperature dependence of the oscillation amplitudes through the standard Lifshitz-Kosevich equation below:

$$\frac{\Delta\rho}{\rho_0} \propto \frac{2\pi^2 k_B m_c T / \hbar e B}{\sinh(2\pi^2 k_B m_c T / \hbar e B)},$$

where $\Delta\rho$ is the oscillation amplitude, ρ_0 is the zero-field resistivity, and k_B is the Boltzmann constant. In electronic systems where several bands are involved, the oscillations are mixed with different frequencies and the cyclotron mass extraction relies on the temperature evolution of amplitudes of the peaks of FFT signal performed over a limited inverse magnetic field window. The fitting of the normalized FFT peak amplitudes by the Lifshitz-Kosevich formula are summarized in Fig. 3(f) and the obtained parameters are listed in Table I. Interestingly, the cyclotron mass m_c shows an obvious trend

TABLE I. Obtained parameters from the analysis of temperature-dependent SdH oscillations. F : oscillation frequency; m_c : cyclotron mass; S_F : FS cross-sectional area; S_F/S_{BZ} : occupation ratio in the first BZ.

Parameters	α	β	γ
F (T)	386 ± 5	574 ± 12	2779 ± 20
m_c (m_e)	0.40 ± 0.02	0.52 ± 0.01	0.83 ± 0.04
S_F (\AA^{-2})	0.0368 ± 0.0005	0.055 ± 0.001	0.265 ± 0.002
S_F/S_{BZ}	$2.52 \pm 0.03\%$	$3.75 \pm 0.08\%$	$18.1 \pm 0.1\%$

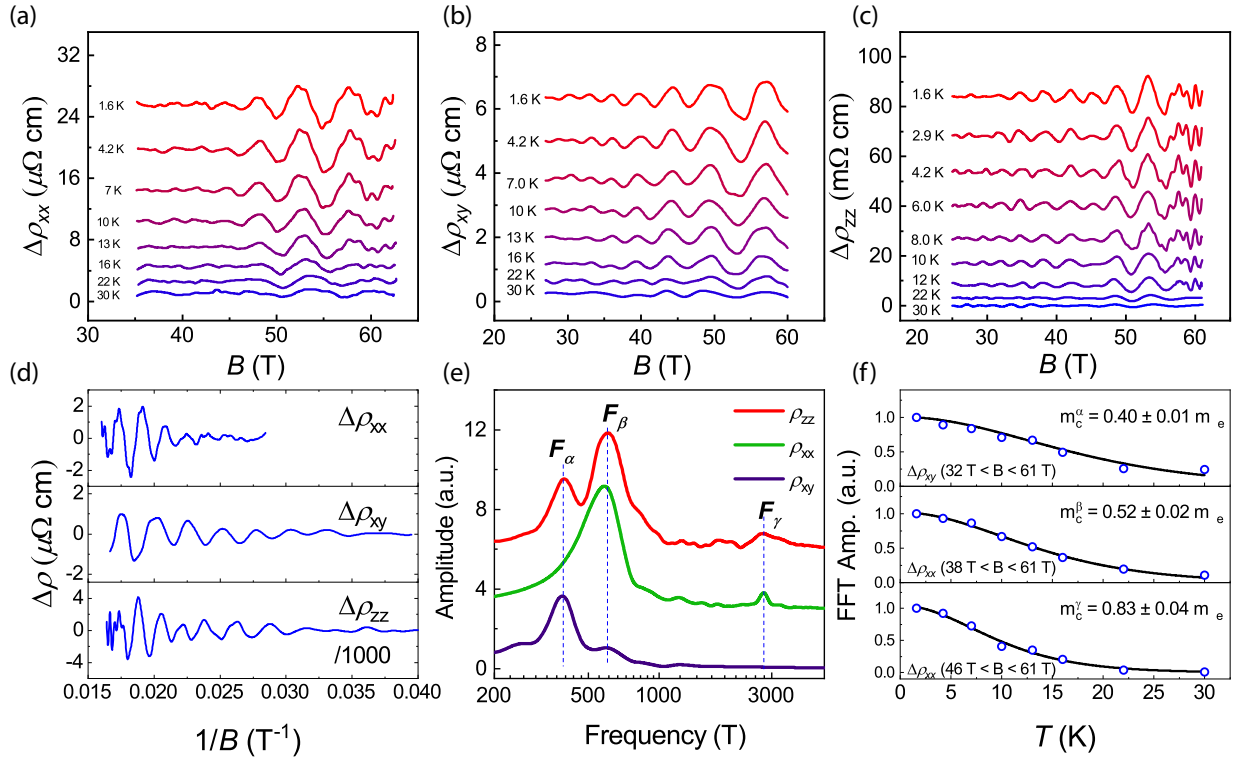


FIG. 3. (a)–(c) The temperature dependence of SdH oscillations of $\Delta\rho_{xx}$, $\Delta\rho_{xy}$, and $\Delta\rho_{zz}$ as a function of magnetic field B after background subtraction by polynomial fits. Curves are shifted for clarity. (d) $\Delta\rho_{xx}$, $\Delta\rho_{xy}$, and $\Delta\rho_{zz}$ as a function of the inverse magnetic field $1/B$ at 1.6 K. (e) The FFT spectra of the data shown in (d). (f) The Lifshitz-Kosevich fitting of the temperature dependence of the oscillation FFT amplitudes of F_α , F_β , and F_γ , respectively.

with the frequency, i.e., the higher the frequency (the larger FS cross-sectional area), the heavier the mass.

A particular interest of the quantum oscillation study is the topology of the FSs associated to the oscillations. To establish the dimensionality of the FSs, we performed the angular dependence studies of the out-of-plane MR on sample S2 at 4.2 K. Figure 4(a) shows the ρ_{zz} at various angles with the measurement configuration depicted in the inset. The sample was rotated from $B \parallel I$ (out-of-plane magnetic field) to $B \perp I$ (in-plane magnetic field) with θ being the angle between B and I . The two transitions at B_1 and B_2 shift to higher field and both scale well with the perpendicular component $B \cos\theta$ (see the Supplemental Material). The weak oscillations superimposed on the ρ_{zz} are extracted after careful background subtractions and are shown in Fig. 4(b). A clear shift of the oscillation features towards higher fields can be easily captured as θ increases, accompanied by the quick vanishing of the high-frequency oscillations at high-field range ($B > 55$ T). We performed FFT for the oscillations as a function of $1/B$ at every angle. Figure 4(c) presents the main SdH oscillation frequencies as a function of θ . The three main frequencies F_α , F_β , and F_γ discussed above follow well with the $1/\cos\theta$ relation at low angles, suggesting the two-dimensionality of related FSs. At high angles ($\theta > 57^\circ$), the oscillation frequency deviates from the $1/\cos\theta$ relation and provides a new set of frequencies at 295 T for $\theta = 89^\circ$ and 211 T for $\theta = 67^\circ$. The origin of the anomalous oscillation behavior is still in doubt due to the quasiperiodicity and the irregular shapes. An alternative would be to attribute it to a series of transitions between

subphases due to the quantization of nesting vector result from the interplay of the Pauli effect and the orbital effect [34].

Based on the transitions and the high-field SdH oscillations, a phase diagram of NMO is built and illustrated in Fig. 1(b). The transition at B_2 strongly resembles the so-called “kink transition” in related CDW systems [35–37]. Remarkable hysteretic behavior between the up-sweep and down-sweep is observed at the transition B_2 when the temperature is low (see the Supplemental Material), indicative of a first-order transition under high magnetic field. This “kink transition” has been ascribed to the Pauli effect which drives the system into a CDW/SDW hybrid state with a smaller gap under high field [38]. On the other hand, the transition at B_1 is likely related to an enhancement of nesting along the field direction due to the orbital effect, similar to the low-field anomalies observed in KMO [37]. It is worth mentioning that in KMO, SdH oscillations were also observed under high magnetic fields and only one frequency ~ 600 T was found in the fields up to 60 T [7,37,39]. To further explore the effect of magnetic field on the CDW states and the high-field electronic structures of the two similar compounds, we have extended the MR studies of KMO up to 80 T, shown in Fig. 5. The high-field SdH oscillations reveal two main frequencies of 642 and 2892 T, which are in good agreement with F_β and F_γ in NMO and provide further evidence for the same origins and similar FS structures of the two isostructural compounds.

The SdH oscillations appear in the high-field range after the B_2 transition enables us to construct the FSs in the CDW/SDW hybrid state [Figs. 1(c)–1(e)]. According to the

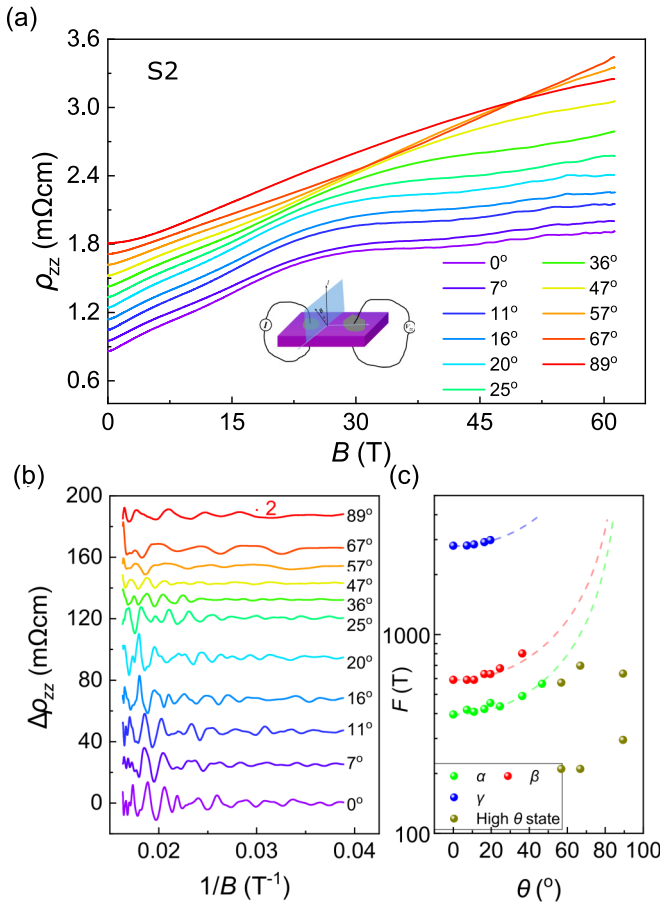


FIG. 4. (a) Angular dependence of the out-of-plane MR ρ_{zz} in sample S2. All the curves are shifted for clarity. The inset shows the measurement configuration. (b) The oscillatory component of ρ_{zz} obtained after subtractions of background at various angles. (c) The angular dependence of the main FFT frequencies of the SdH oscillations. The dashed lines are the fits to the 2D FS model of $F(\theta) = F(0)/\cos\theta$.

theoretical work of Su *et al.* [26], the CDW formation gaps out most of the FSs and only small arclike electron and hole pockets remain at the M' point in the unfolded BZ [shown in Fig. 1(c)]. In the case of another molybdenum purple bronze η - Mo_6O_{11} , the remaining FS pockets contribute to SdH oscillations under very low fields with frequencies ranging from 2.5 to 20 T [40]. The slow oscillations with frequencies F_α and F_β in NMO are thus believed not to originate from the arclike electron and hole pockets at M' remaining in the CDW state, taking into account the large cross-sectional areas of the α and β pockets. As mentioned above, the α oscillations are only observed on ρ_{xy} with negative background under high field. Generally, the high-field ρ_{xy} is mainly dominated by the highest mobility carrier in a multiband system, as well as the oscillations on it [41]. Therefore we can easily conclude that α correspond to the electronlike pockets around the M' point. The light cyclotron mass of the α pockets can be explained by the weakest electron-phonon coupling at the M' point where the least FS nesting occurs. On the other hand, the pockets of β are attributed to holelike for the following reason. In KMO, SdH oscillations are also observed both on ρ_{xx} and ρ_{xy} with

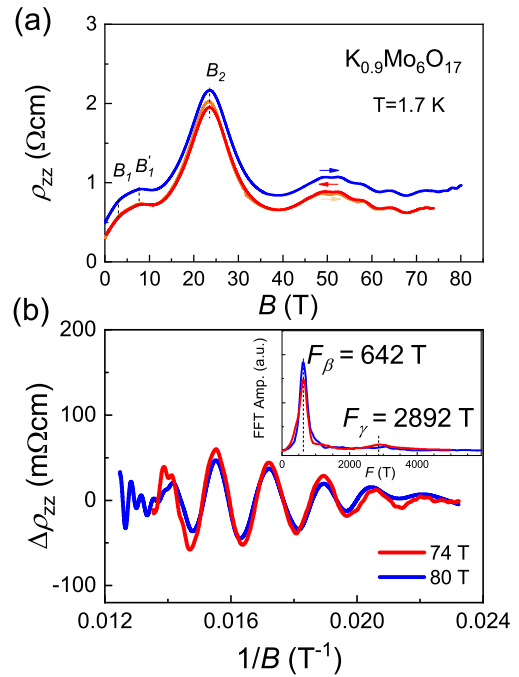


FIG. 5. (a) The out-of-plane resistivity ρ_{zz} of $\text{K}_{0.9}\text{Mo}_6\text{O}_{17}$ during two shots up to 74 and 80 T, respectively. The arrows indicate the field sweep direction. Only the data during up-sweep of the 80 T pulse was captured. (b) The oscillation components $\Delta\rho_{zz}$ of the two shots and the FFT spectra (inset). Two main peaks are revealed at 642 and 2892 T, respectively.

only one frequency around 600 T up to 60 T [7,37,39]. The cyclotron mass of the oscillations was extracted to be around $0.6m_e$, very close to that of the β frequency oscillations in NMO ($0.52m_e$). The similarities of the frequency and the cyclotron mass in the two compounds really suggest the same origin of the oscillations. From the positive ρ_{xy} of KMO, it is reasonable to assume the β oscillations in NMO originate from hole pockets which also reside near the M' point. A possible FS structure is proposed and sketched in Fig. 1(d) under high magnetic field. The orange area corresponds to the electron pockets and blue parts correspond to hole pockets, which have been enlarged from the remaining arclike electron and hole pockets in the CDW state by the effect of magnetic field. We expect that the Pauli term under high magnetic field shifts the bands of different spins and induces a poorer nesting, driving the system to a suppressed CDW state with more FS segments recovered. Further, we notice that the highest frequency F_γ corresponds to a cross-sectional area occupying 18.1% of the unfolded first Brillouin zone (FBZ) of NMO at high temperatures. This large area is perfectly consistent with the FS of the inner hexagonal electron whose Fermi wave vector was measured to be $0.52 \Gamma M$ by ARPES in the normal state [29]. The appearance of the fast oscillations can be ascribed to the magnetic breakdown between the six electron pockets denoted as α . The cyclotron mass shows a pronounced enhancement from $0.4m_e$ of the α pocket to $0.83m_e$ of the γ orbit due to the higher density of state of the original electron hexagonal FS of the normal state [Fig. 1(e)]. On the other hand, the breakdown of the β hole pockets is still unobservable at present experimental conditions since the

outer orbits possess even higher effective mass than the inner γ orbit.

IV. CONCLUSION

To conclude, we have studied in detail the magnetotransport properties of quasi-two-dimensional CDW systems of $A_{0.9}\text{Mo}_6\text{O}_{17}$ ($A = \text{K}, \text{Na}$) under high magnetic fields. The temperature dependence of the in-plane and out-of-plane resistivity show typical CDW transitions at $T_{\text{CDW}} = 85$ K of $\text{Na}_{0.9}\text{Mo}_6\text{O}_{17}$. Pronounced SdH oscillations have been observed under high magnetic field at low temperature. The FFT spectra of the oscillations reveal three frequencies in ρ_{xx} , ρ_{xy} , and ρ_{zz} . Angular studies of the SdH oscillations suggest the 2D properties of the related FSs and further possible transitions induced by the interplay between the Pauli coupling and the orbital effect at high angles and under high fields. The

analyses of the SdH oscillations enable us to build the phase diagram and construct the FS structure of NMO. The observation of a fast oscillation which corresponds to a FS cross section occupying 18.1% of the FBZ of the normal state strongly suggests the magnetic breakdown under high field in this system. This magnetic breakdown behavior has also been observed in KMO under a much higher magnetic field up to 80 T.

ACKNOWLEDGMENTS

This work is supported by the National Key Research and Development Plan Project of China (Grant No. 2016YFA0401700), the National Natural Science Foundation of China (Grants No. 12004122, No. U1832214, No. 51821005, and No. U1732162) and the Fundamental Research Funds for the Central Universities (No. 2018KFYXKJC005 and No. 2019kfyXJJ009).

-
- [1] G. Grüner, *Rev. Mod. Phys.* **60**, 1129 (1988).
- [2] M. Greenblatt, K. V. Ramanujachary, W. H. McCarroll, R. Neifeld, and J. V. Waszczak, *J. Solid State Chem.* **59**, 149 (1985).
- [3] M. H. Whangbo, E. Canadell, and C. Schlenker, *J. Am. Chem. Soc.* **109**, 6308 (1987).
- [4] A. Rötger, J. Dumas, J. Marcus, C. Schlenker, J. Ulmet, A. Audouard, and S. Askenazy, *Physica B* **177**, 318 (1992).
- [5] P. Mallet, K. M. Zimmermann, P. Chevalier, J. Marcus, J. Y. Veuillen, and J. M. Gomez Rodriguez, *Phys. Rev. B* **60**, 2122 (1999).
- [6] H. Guyot, J. Dumas, M. V. Kartsovnik, J. Marcus, C. Schlenker, I. Sheikin, and D. Vignolles, *Eur. Phys. J. B* **58**, 25 (2007).
- [7] J.-F. Wang, M. Yang, L. Li, M. Sasaki, A. Ohnishi, M. Kitaura, K.-S. Kim, and H.-J. Kim, *Phys. Rev. B* **89**, 035137 (2014).
- [8] M. H. Whangbo, E. Canadell, P. Foury, and J. P. Pouget, *Science* **252**, 96 (1991).
- [9] H. Cercellier, C. Monney, F. Clerc, C. Battaglia, L. Despont, M. G. Garnier, H. Beck, P. Aebi, L. Patthey, H. Berger, and L. Forró, *Phys. Rev. Lett.* **99**, 146403 (2007).
- [10] C. J. Arguello, S. P. Chockalingam, E. P. Rosenthal, L. Zhao, C. Gutiérrez, J. H. Kang, W. C. Chung, R. M. Fernandes, S. Jia, A. J. Millis, R. J. Cava, and A. N. Pasupathy, *Phys. Rev. B* **89**, 235115 (2014).
- [11] X. Zhu, Y. Cao, J. Zhang, E. W. Plummer, and J. Guo, *Proc. Natl. Acad. Sci. USA* **112**, 2367 (2015).
- [12] K. Rossnagel, *J. Phys.: Condens. Matter* **23**, 213001 (2011).
- [13] P. Knowles, B. Yang, T. Muramatsu, O. Moulding, J. Buhot, C. J. Sayers, E. Da Como, and S. Friedemann, *Phys. Rev. Lett.* **124**, 167602 (2020).
- [14] J. Chang, E. Blackburn, A. T. Holmes, N. B. Christensen, J. Larsen, J. Mesot, R. Liang, D. A. Bonn, W. N. Hardy, A. Watenphul, M. v. Zimmermann, E. M. Forgan, and S. M. Hayden, *Nat. Phys.* **8**, 871 (2012).
- [15] S. Gerber, H. Jang, H. Nojiri, S. Matsuzawa, H. Yasumura, D. A. Bonn, R. Liang, W. N. Hardy, Z. Islam, A. Mehta, S. Song, M. Sikorski, D. Stefanescu, Y. Feng, S. A. Kivelson, T. P. Devereaux, Z. X. Shen, C. C. Kao, W. S. Lee, D. Zhu, and J. S. Lee, *Science* **350**, 949 (2015).
- [16] X. Xu, A. F. Bangura, J. G. Analytis, J. D. Fletcher, M. M. J. French, N. Shannon, J. He, S. Zhang, D. Mandrus, R. Jin, and N. E. Hussey, *Phys. Rev. Lett.* **102**, 206602 (2009).
- [17] J.-F. Mercure, A. F. Bangura, X. Xu, N. Wakeham, A. Carrington, P. Walmsley, M. Greenblatt, and N. E. Hussey, *Phys. Rev. Lett.* **108**, 187003 (2012).
- [18] F. Wang, J. V. Alvarez, S.-K. Mo, J. W. Allen, G.-H. Gweon, J. He, R. Jin, D. Mandrus, and H. Höchst, *Phys. Rev. Lett.* **96**, 196403 (2006).
- [19] P. Chudzinski, T. Jarlborg, and T. Giamarchi, *Phys. Rev. B* **86**, 075147 (2012).
- [20] J. Lu, X. Xu, M. Greenblatt, R. Jin, P. Tinnemans, S. Licciardello, M. R. van Delft, J. Buhot, P. Chudzinski, and N. E. Hussey, *Sci. Adv.* **5**, eaar8027 (2019).
- [21] N. Wakeham, A. F. Bangura, X. Xu, J.-F. Mercure, M. Greenblatt, and N. E. Hussey, *Nat. Commun.* **2**, 396 (2011).
- [22] M. Greenblatt, *Chem. Rev.* **88**, 31 (1988).
- [23] X. Xu, A. F. Bangura, C. Q. Niu, M. Greenblatt, S. Yue, C. Panagopoulos, and N. E. Hussey, *Phys. Rev. B* **85**, 195101 (2012).
- [24] M. A. Valbuena, J. Avila, D. V. Vyalikh, H. Guyot, C. Laubschat, S. L. Molodtsov, and M. C. Asensio, *J. Phys.: Conf. Ser.* **100**, 072021 (2008).
- [25] D. Mou, A. Sapkota, H.-H. Kung, V. Krapivin, Y. Wu, A. Kreyssig, X. Zhou, A. I. Goldman, G. Blumberg, R. Flint, and A. Kaminski, *Phys. Rev. Lett.* **116**, 196401 (2016).
- [26] L. Su, C.-H. Hsu, H. Lin, and V. M. Pereira, *Phys. Rev. Lett.* **118**, 257601 (2017).
- [27] K. Breuer, C. Stagescu, K. E. Smith, M. Greenblatt, and K. Ramanujachary, *Phys. Rev. Lett.* **76**, 3172 (1996).
- [28] G. H. Gweon, J. W. Allen, J. A. Clack, Y. X. Zhang, D. M. Poirier, P. J. Benning, C. G. Olson, J. Marcus, and C. Schlenker, *Phys. Rev. B* **55**, R13353(R) (1997).
- [29] P.-A. Glans, T. Learmonth, K. E. Smith, T. Valla, P. D. Johnson, S. L. Hulbert, W. McCarroll, and M. Greenblatt, *Phys. Rev. B* **72**, 035115 (2005).

- [30] K. Ramanujachary, M. Greenblatt, and W. McCarroll, *J. Cryst. Growth* **70**, 476 (1984).
- [31] See Supplemental Material at <http://link.aps.org/supplemental/10.1103/PhysRevB.102.235164> for details of the comparison of the up-sweep and down-sweep, the second derivatives of ρ_{xx} , the temperature-dependent FFT, and the pulse of the 80 T data.
- [32] M. Tian, S. Yue, and Y. Zhang, *Phys. Rev. B* **65**, 104421 (2002).
- [33] D. Shoenberg, *Magnetic Oscillations in Metals*, Cambridge Monographs on Physics (Cambridge University Press, Cambridge, UK, 1984).
- [34] D. Andres, M. V. Kartsovnik, P. D. Grigoriev, W. Biberacher, and H. Müller, *Phys. Rev. B* **68**, 201101(R) (2003).
- [35] C. Proust, A. Audouard, A. Kovalev, D. Vignolles, M. Kartsovnik, L. Brossard, and N. Kushch, *Phys. Rev. B* **62**, 2388 (2000).
- [36] J. S. Qualls, L. Balicas, J. S. Brooks, N. Harrison, L. K. Montgomery, and M. Tokumoto, *Phys. Rev. B* **62**, 10008 (2000).
- [37] J. Dumas, H. Guyot, H. Balaska, J. Marcus, D. Vignolles, I. Sheikin, A. Audouard, L. Brossard, and C. Schlenker, *Phys. B (Amsterdam, Neth.)* **346**, 314 (2004).
- [38] D. Zanchi, A. Bjeliš, and G. Montambaux, *Phys. Rev. B* **53**, 1240 (1996).
- [39] H. Balaska, J. Dumas, H. Guyot, P. Mallet, J. Marcus, C. Schlenker, J. Veuillen, and D. Vignolles, *Solid State Sci.* **7**, 690 (2005).
- [40] S. Hill, S. Valfells, S. Uji, J. S. Brooks, G. J. Athas, P. S. Sandhu, J. Sarrao, Z. Fisk, J. Goettee, H. Aoki, and T. Terashima, *Phys. Rev. B* **55**, 2018 (1997).
- [41] M. D. Watson, T. Yamashita, S. Kasahara, W. Knafo, M. Nardone, J. Béard, F. Hardy, A. McCollam, A. Narayanan, S. F. Blake, T. Wolf, A. A. Haghighirad, C. Meingast, A. J. Schofield, H. v. Löhneysen, Y. Matsuda, A. I. Coldea, and T. Shibauchi, *Phys. Rev. Lett.* **115**, 027006 (2015).

Correction: The previously published Figure 5(b) contained an error in the curve key and has been replaced.